

that produced by much wetter years prior to 1970 suggests that the general recent tendency of increased high water levels is largely independent of precipitation and thus is more likely related to the changes in drainage and runoff associated with deforestation.

Thus, the irreversible changes in Amazonian water balance predicted by Sioli (12) seem already to have begun. Increased settlement in upper Amazonia, where richer soils lessen the agricultural constraints imposed on much of central and lower Amazonia, could result in increased annual flooding and economic and ecological damage thousands of kilometers away in central and lower Amazonia. Since most of Amazonia's population and agriculture are concentrated along the seasonally flooded strip immediately adjacent to the main river, the magnitude of the damage is potentially great.

According to current predictions, present rates of forest destruction will result in elimination of tropical rainforest from the face of the earth not long after the turn of the century (3, 18). However, most of the Amazonian rain forest remains uncut at this moment. The rapidity with which relatively limited forest destruction appears already to have altered the Amazonian water balance, suggests the need for planned development that takes into account this delicate ecological balance.

A. H. GENTRY

Missouri Botanical Garden,
Post Office Box 299, St. Louis 63166

J. LOPEZ-PARODI

Proyecto PARI Jenaro Herrera,
Iquitos, Peru

References and Notes

1. R. Greswell and A. Huxley, Eds., *Standard Cyclopedia of the World's Rivers and Lakes* (Weidenfeld and Nicholson, London, 1964).
2. H. Sioli, in *River Ecology*, B. Whitton, Ed. (Blackwell, London, 1975), pp. 461-488.
3. *Conversion of Tropical Moist Forest* (National Academy of Sciences, Washington, D.C., 1980), pp. 1-240.
4. A. Sommer, *Unasylva* 28, 5 (1976); A. Gentry, in *Systematic Botany, Plant Utilization and Biosphere Conservation*, I. Hedberg, Ed. (Almqvist and Wiksell, Stockholm, 1979), pp. 110-130.
5. M. Douroujeanni, *Rev. For. Peru* 6, 41 (1976); typescript, 1979, cited in (3).
6. J. Kirby, *Pac. Viewpoint* 17, 105 (1976); Anonymous, *Atlas Geografico del Ecuador* [Instituto Geografico Militar, Quito (without date)].
7. J. W. Terborgh, *Ecology* 52, 23 (1971); _____ and T. R. Dudley, *Natl. Geogr. Soc. Res. Rep.* (National Geographic Society, Washington, D.C., 1976), pp. 255-264; K. Wehr, personal communication.
8. A. D. Putney, *Estrategia preliminar para conservación de áreas silvestres sobresalientes del Ecuador*, UNDP/FAO-ECU/71/527; A. Gentry, in *Extinction Is Forever*, G. Prance and T. Elias, Eds. (New York Botanical Garden, New York, 1977), pp. 136-149.
9. C. Sagan, O. Toon, J. Pollack, *Science* 206, 1363 (1979).
10. H. Lamprecht, in *Ecosystem Research in South America*, P. Muller, Ed. (Junk, The Hague, 1977), pp. 1-16; L. S. Hamilton, J. Steyermark, J. P. Veillon, E. Mundolfi, *Conservación de los bosques húmedos de Venezuela* (Sierra Club-

- Consejo de Bienestar Rural, Caracas, 1976).
11. E. Saletti, J. Barques, L. C. Molion, *Interciencia* 3, 200 (1978).
 12. H. Sioli, in *Tropical Ecological Systems: Trends in Terrestrial and Aquatic Research*, F. B. Golley and E. Medina, Eds. (Springer-Verlag, New York, 1975), pp. 275-288; in *Landscape Ecology*, P. Muller and C. Rathjens, Eds. (Biogeographica No. 16, Kluwer Boston, Hingham, Mass., 1980), pp. 145-158.
 13. R. J. Goodland and H. S. Irwin, *Amazon Jungle: Green Hell to Red Desert* (Elsevier, New York, 1975).
 14. V. Kovda, in *Okologie und Lebensschutz in Internationaler Sicht—Ecology and Bioprotection, International Conclusions*, H. Sioli, Ed. (Rombach, Freiburg, 1973), pp. 63-89; H. Sioli, paper presented at Conference on the Development of Amazonia in Seven Countries, Cambridge University, Cambridge, England, 1979.
 15. H. Sioli, personal communication.
 16. The observed trend in increasingly high floods could also be explained as a result of progressive silting of the Amazon as suggested by P. le Coite [Bol. Mus. Para. Emilio Goeldi 10, 177 (1948)] and L. Soares [Rev. Bras. Geogr. 16, 397

(1954)], a suggestion disproved by H. O. Sternberg [thesis, Faculdade Nacional de Filosofia da Universidade do Brasil, Rio de Janeiro (1956)]; H. Sternberg, personal communication.

17. Precipitation data for Peruvian Amazonia are incomplete, and no reporting station has complete data for all the years covered by the river level records. Only years with complete data were used in compiling and analyzing totals for each station.
18. P. Raven, *Frontiers* 40, 22 (1976); P. Richards, *Sci. Am.* 229, 58 (1973).
19. Anonymous, *Inventario, Evaluación e Integración de los Recursos Naturales de la Selva, Zona Iquitos, Nauta, Requena y Colonia Angamos* (ONERN, Lima, 1976).
20. We thank G. Prance, P. Raven, H. Sioli, and N. Myers for criticism of the manuscript or providing relevant information, C. Diaz and H. de Diaz for compiling part of the river level data from the raw records, and ONERN for making available the rainfall data. Supported by grants from the National Science Foundation and National Geographic Society.

16 January 1980; revised 5 June 1980

Chemical Species in Fly Ash from Coal-Burning Power Plants

Abstract. Fly ash specimens from four power plants in the Tennessee Valley Authority system have been separated into three matrices: glass, mullite-quartz, and magnetic spinel. Chemical species of trace elements are defined to a large extent by the matrices that contain them. The magnetic component of fly ash is ferrite. The mullite-quartz phase is relatively pure and can be recovered as a resource.

We have studied fly ash specimens from the Kingston, Bull Run, Johnsonville, and Paradise plants in the Tennessee Valley Authority system. Specimens were taken from electrostatic precipitators and cyclone devices. Firing characteristics and coal sources have been described (1, 2). Each of the ashes was size-fractionated and magnetically separated. Aluminosilicate materials were sintered to the magnetic particles, which prevented a complete separation by physical means. The magnetic fractions were then treated with concentrated HCl, which dissolved most of the iron-containing spinels and oxides, leaving the aluminosilicate materials as residue. Glass phases were removed from the nonmagnetic phases by etching in 1 percent HF. This separation is believed to be effected by differences in dissolution rates; the glass phases dissolve rapidly, whereas the crystalline mullite and quartz react much more slowly. A weight loss curve showing the kinetics of the glass removal is discussed in (2). The residue that remained consisted of mullite and quartz skeletons of the original particles. Thus we have separated each of the fly ash specimens into its three main matrices: glass, mullite-quartz, and magnetic spinel. These have been individually characterized and analyzed for trace element distributions (Table 1). Because of space limitations, only the results for the Bull Run plant are given here. Compositions for the other three plants were very similar.

Before discussing the trace element distributions, let us consider the nature of the matrices that contained them. If we represent the glass phases as $(\text{SiO}_2)_x \cdot (\text{R}_2\text{O}_3)_y$, where R is Al or Fe, we find from Table 1 that $x/y \approx 11/2$ for the Bull Run ash. For the other three ashes, x/y varied between 9/2 and 14/2. Figure 1 shows scanning electron micrographs of the mullite and quartz phases left after the glasses had been extracted with 1 percent HF. Clusters of acicular mullite crystallites are shown in Fig. 1, a, b, and c. Their spherical symmetries reflect the original shapes of the ash particles before etching. The glass phases that were removed occupied interstitial positions between the needle crystallites. Figure 1d shows a quartz skeleton remaining after the glass phases have been etched away. The identities of the particles in Fig. 1 have been established by means of x-ray fluorescence induced by the beam of the scanning electron microscope and by x-ray diffraction. Analytical results for individual acicular mullite crystals varied by as much as 20 percent for the four ashes studied, but the compositions were approximately that of the natural mineral, $3(\text{Al}_2\text{O}_3) \cdot 2(\text{SiO}_2)$. Quartz phases such as that in Fig. 1d contained Al concentrations ranging between 2 and 10 percent (by weight). Table 1 shows that the magnetic material extracted by HCl contained an appreciable amount of Al and Fe. We take this to mean that the magnetic spinel material in fly ash is ferrite, rather than magnet-

ite, as commonly reported. The composition of this ferrite material is approximately $Fe_{2.3}Al_{0.7}O_4$. X-ray diffraction patterns of the magnetic fractions of the fly ash specimens showed the same symmetry as that of Fe_3O_4 , but the lattice constants were too small (2) to be accounted for by this compound. If we assume that Al is isomorphically substituted for Fe, the shrinkage of the lattice can be explained. X-ray diffraction patterns showed that crystalline Al_2O_3 was not present in either the magnetic or the nonmagnetic phase. Small amounts (10 percent) of $\alpha-Fe_2O_3$ were found in the magnetic phases.

The data in Table 1 show preferential distributions in trace element contents for the three matrices. If we compare the two nonmagnetic components, we can see that the alkali, rare-earth, and many transition elements are more concentrated in the glass phase than in the mullite-quartz phase. The only elements consistently more concentrated in the mullite-quartz phase than in the glass phase for all ashes studied were Cr and Ga; V was distributed equally between these two phases. The data show that, with the exception of Mg and Ca, all monovalent and divalent metals are more concentrated in the glass. The Mg and Ca vagaries in the mullite phase are artifacts of the HF extraction process (2). The first-row transition elements—V, Cr, Mn, Co, Ni, Zn, and Cu—are more concentrated in the magnetic phase. The high concentrations of Na, K, and Rb in the HCl-extracted magnetic phases may be due to their presence as soluble silicates. Trace element distributions, as well as the compositions of the matrix materials, were qualitatively the same for all four ashes. This result suggests that the structure of fly ash and the species of its elements are independent of coal source and firing conditions. We hesitate to make the generalization for all ashes, especially since we have not studied those of western U.S. coals, but for eastern Tennessee and western Kentucky sources burned in conventional steam plants it seems to be true.

The data in Table 1 are in support of our thesis that chemical species of trace elements are defined by the matrices in which they are dissolved. Since most of the trace elements of high concentration in the mullite-quartz phase have valences of either +3 or +4, they are probably contained in the mullite crystalline lattice as isomorphous substitutions for Al and Si. Their ionic radii are sufficiently small to allow this. In the magnetic phase, the elements V, Cr, Mn, Co, Ni, and Zn are probably in the form of sub-

stituted spinels, $Fe_{3-x}M_xO_4$. Perhaps La and Ce are also incorporated in this way. In nonmagnetic aluminosilicate components, the glass phases contain most of the potentially toxic trace elements.

From our results we derive conclusions pertaining to three aspects of fly ash: (i) the mechanism of formation, (ii) long-term leaching behavior, and (iii) resource recovery. By examining microstructures and measuring element distri-

Table 1. Element distributions (in parts per million) in the 100- to 200- μ m fraction of Bull Run fly ash.

Element	Glass	Mullite-quartz	Magnetic spinel (HCL-extracted)	Element	Glass	Mullite-quartz	Magnetic spinel (HCL-extracted)
Al	87,200	204,000	86,600	Ga	0	12	0
Fe	19,600	3,400	605,000	As	42	2	0
Si	343,000	287,000		Se	54	7	38
Na	1,710	256	2,080	Mo	0	3	0
K	25,000	5,270	3,590	Cd	0.32	0.27	1.2
Rb	532	12	229	Hf	6	3	0
Cs	0	0	0	Ta	3	1	0
Mg	10,400	15,500	0	W	4	1	0
Ca		0	0	Hg	8	1	0
Sr	798	174	0	Pb	35	2	
Ba	319	69	0	La	61	0	14
Sc	31	7	15	Ce	119	6	141
Ti	10,900	4,630	0	Sm	0	0	0
V	176	127	150	Eu	2	0	1
Cr	169	311	1,380	Tb	5	0	0
Mn	87	9	1,040	Dy	10	0	0
Co	25	2	251	Yb	4	0	0
Ni	174	78	2,270	Th	5	0	5
Cu	144	17	496	U	13	1	4
Zn	209	17	382				

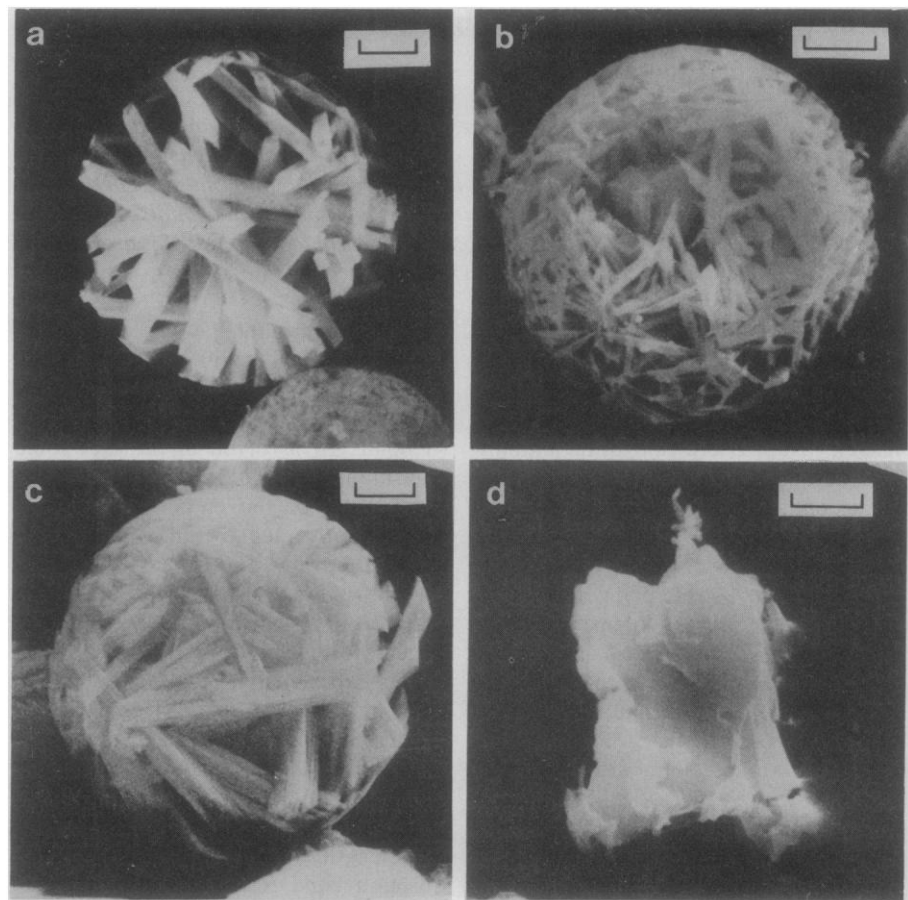


Fig. 1. Skeletons of fly ash particles remaining after etching in 1 percent HF: (a, b, and c) clusters of acicular mullite crystals; (d) a quartz particle. Each scale bar is 2 μ m.

bution patterns, we find that the qualitative nature of fly ash as independent of coal source and firing conditions. This suggests that the ashes are in near-equilibrium states rather than as frozen transients. Growth of the mullite crystallites occurs over several micrometers (Fig. 1). This means that there was time for the trace elements to be frozen out and concentrated in the glass phases. Perhaps the segregation of trace elements at fly ash surfaces, reported by Linton *et al.* (3) and Smith *et al.* (4), occurs by transport from the inside of the particle as well as by condensation from the vapor phase. The Gibbs adsorption isotherm states that the surface free energy of liquids decreases when solutes migrate to the surface. Long-term leaching behavior occurs primarily in glass and magnetic spinel matrices. It appears to us that, if the magnetic phases are removed from fly ash specimens before they are buried, the amount of leaching and runoff from first-row transition elements would diminish. Pollution from Cr and Ni should be especially reduced. The Cr in the nonmagnetic phase is trapped in the mullite lattice that should

be more inert to breakdown. It appears to us that the mullite and quartz present in fly ash may be a valuable resource. As much as 30 percent of the nonmagnetic fraction is in this form. Mullite is a widely marketed refractory ceramic used for making china, electrical insulators, and high-temperature devices. Mullite is presently made by the mining and firing of kaolinite, which is an energy-intensive process. Perhaps the chemical refinement of mullite and quartz already present in fly ash has economic merit.

L. D. HULETT, JR., A. J. WEINBERGER
K. J. NORTHCUTT, MARIAN FERGUSON
*Oak Ridge National Laboratory,
Oak Ridge, Tennessee 37830*

References and Notes

1. L. D. Hulett and A. J. Weinberger, *Environ. Sci. Technol.* **14**, 965 (1980).
2. ———, N. M. Ferguson, K. J. Northcutt, W. S. Lyon, Report RP 1061 (Electric Power Research Institute, Palo Alto, Calif., July 1979).
3. R. W. Linton, P. Williams, C. A. Evans, D. F. S. Natusch, *Anal. Chem.* **49**, 1514 (1977).
4. R. D. Smith, J. A. Campbell, K. K. Nielson, *J. Am. Chem. Soc.* **101**, 553 (1979).
5. We thank the Tennessee Valley Authority for supplying ash samples. We appreciate the expert guidance in photography given by J. W. Jones. Research supported by the Electric Power Research Institute, Palo Alto, Calif.

14 February 1980; revised 14 July 1980

Resonance Raman Effect of Carbonyl Group as a Probe of Its π -Electron State

Abstract. By examining the occurrence or absence of a resonance Raman effect for a carbonyl bond-stretching vibration, one can achieve a unique characterization of the carbonyl π -electrons. It can be concluded, for example, that the carbonyl π -electrons of nicotinamide do not migrate into the ring π -electron orbitals responsible for the 265-nanometer band, whereas those of dihydronicotinamide do migrate into orbitals responsible for the 340-nanometer band.

The Raman line caused by a carbonyl stretching vibration is often strong and is usually identified with high reliability, even in a complex compound such as a nucleic acid, a coenzyme, or an antibiotic. The question may be raised, Under what condition is a carbonyl stretching vibration involved in a resonance Raman effect? As an answer we suggest a simple rule: A carbonyl stretching vibration will show greatly enhanced intensity in a resonance Raman spectrum from a given excited electronic state if the state is a $\pi\pi^*$ transition of a conjugated double-bond system and if the carbonyl bond in question is involved in the conjugated system.

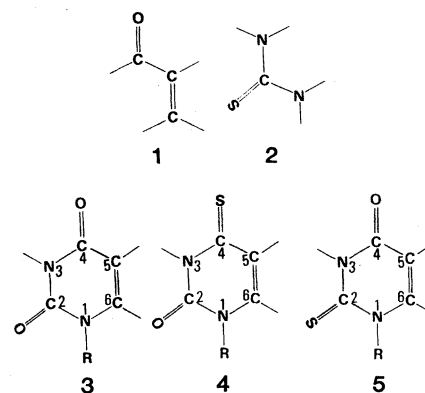
This rule is an extension of one published by Hirakawa and Tsuboi (1), which stated that, if there is a change in the molecular geometry in the excited electronic state that mirrors a normal

mode of the ground-state molecule, then that normal mode will be active in the resonance Raman spectrum. In the present case, if the π -electrons in the carbonyl bond are involved in the electronic transition, there will be a decrease in the bond order of the carbonyl bond and consequently a lengthening of that bond. We will review experimental evidence for the rule and give some examples to show how it is useful in the present, less general form.

Our experimental results are summarized in Table 1. A resonance Raman effect is most reliably detected by examination of a Raman excitation profile. If, in a curve of the intensity I_j of a Raman line j plotted against the excitation wavelength λ_{exc} , a peak appears in an absorption band $\tilde{N} \leftarrow \tilde{X}$, it is concluded that j is in resonance with $\tilde{N} \leftarrow \tilde{X}$. The same conclusion is often drawn merely

by observing a well-defined Raman line with an excitation wavelength in the $\tilde{N} \leftarrow \tilde{X}$ band. If the molar extinction coefficient for λ_{exc} is 10^3 to 10^4 , the sample concentration (in an aqueous solution, for example) for the Raman scattering measurement is usually 10^{-3} to $10^{-4}M$. The fact that a distinct Raman line is observed for such a dilute sample solution is taken as an evidence of the resonance Raman effect.

In acrolein (1), the Raman scattering intensity of the C=O stretching vibration at 1693 cm^{-1} increases monotonously on changing λ_{exc} from 363.8 to 290 nm. It is concluded that the C=O Raman line is not in resonance with the 340-nm band [$n\pi^*$ transition of the O=C-C=C system (2)], but it probably is in resonance with the 197-nm band ($\pi\pi^*$ transition). The 250-nm band of thiourea (2) is essentially the longest wavelength $\pi\pi^*$ transition (3), and the C=S stretching Raman line is in resonance with this band (4). The uracil residue (3) has two C=O stretching vibrations. The 1720-cm^{-1} line (C²=O) is not in resonance with the 260-nm band, whereas the 1680-cm^{-1} line (C⁴=O) is in resonance (5). The electrons associated with the 260-nm band ($\pi\pi^*$) are known to be localized in the O=C⁴-C⁵=C⁶ part of the molecule, and the C²=O bond is not considered to be involved in the conjugated double-bond system (6, 7). These observations are considered to form evidence for the rule stated above. This interpretation is supported by the fact that the 4-thiouracil residue (4) has a C=O stretching vibration (1700 cm^{-1}) that is not in resonance with its 333-nm band, whereas the 2-thiouracil residue (5) has a C=O Raman line (1690 cm^{-1}) that is in resonance with its 300-nm band.



The rule can be used to judge whether a particular carbonyl group is involved in a conjugated double-bond system. Even when a C=O bond appears, from the structural formula, to be conjugated with a C=C (or C=N) bond, the π -electrons